PHYSICAL REVIEW A **92**, 060501(R) (2015)

Measurement of Rb $5P_{3/2}$ scalar and tensor polarizabilities in a 1064-nm light field

Yun-Jhih Chen,[1] Luís Felipe Gonçalves,[1,2] and Georg Raithel[1]
[1]*Department of Physics, University of Michigan, Ann Arbor, Michigan 48109, USA*
[2]*Instituto de Física de São Carlos, Universidade de São Paulo, Caixa Postal 369, 13560-970, São Carlos, SP, Brasil*
(Received 28 July 2015; published 9 December 2015)

We employ doubly resonant two-photon excitation into the $74S$ Rydberg state to spectroscopically measure the dynamic scalar polarizability, α_0, and tensor polarizability, α_2, of rubidium $5P_{3/2}$. A cavity-generated 1064-nm optical lattice allows us to reach intensities near 2×10^{11} W/m^2, where the atom field is larger than the hyperfine interaction, and magnetic sublevels are well resolved. In the evaluation of the data we use a self-referencing method that renders the polarizability measurement largely free from the intensity calibration of the laser light field. We obtain experimental values $\alpha_0 = -1149(\pm 2.5\%)$ and $\alpha_2 = 563(\pm 4.2\%)$, in atomic units. Methods and results are supported by simulations. The results provide an experimental test of atomic-structure calculations used to determine systematic shifts in atomic clocks and to interpret fundamental-physics experiments.

DOI: 10.1103/PhysRevA.92.060501 PACS number(s): 32.10.Dk, 42.50.Hz, 37.10.Jk, 37.30.+i

Polarizabilities of atomic energy levels govern the response of an atom to an external electric field and are essential in atom trapping and high-precision measurement. Theoretical calculations of dynamic polarizabilities are complicated, and yet available experimental measurements might carry large uncertainties due to the difficulty in calibrating the field strength experienced by the atoms. Here, we report a measurement of rubidium scalar and tensor polarizabilities conducted in a strong 1064-nm light field, where the magnetic sublevels of Rb $5P_{3/2}$ are resolved and the data analysis is largely free from the calibration of laser intensity. Our work is not only applicable to experiments utilizing Rb $5P_{3/2}$ levels in 1064-nm laser traps, but also serves as an experimental test for validating and improving existing theoretical models for the polarizability, where complex Dirac-Fock atomic-structure calculations are employed to derive the required matrix elements [1–3]. Experimental tests are valuable even if they are performed only at specific wavelengths. Accurate and precise information on light and blackbody shifts, obtained from a combination of theoretical and experimental work, is necessary, for instance, to determine magic wavelengths for state-insensitive trapping in optical lattices [4,5], to characterize blackbody shifts in optical atomic clocks [2] and to interpret atomic parity nonconservation experiments [1,3].

In the presence of an optical field, an atom is polarized and its energy levels are shifted. The atom-field interaction Hamiltonian, $\hat{H}_{\rm E}$, in a linearly polarized electric field with amplitude E_0 is

$$-\frac{E_0^2}{4}\sum_{m_J}|J,m_J\rangle\langle J,m_J|\left[\alpha_0+\alpha_2\frac{3m_J^2-J(J+1)}{J(2J-1)}\right], \quad (1)$$

where $\alpha_0(\omega)$ and $\alpha_2(\omega)$ are frequency-dependent ac scalar and tensor polarizabilities, and J and m_J are electronic angular-momentum quantum numbers. For Rb $5S_{1/2}$ it is $\alpha_2 = 0$, while for $5P_{3/2}$ both α_0 and α_2 contribute to the polarizability. The full Hamiltonian includes the hyperfine structure, $\hat{H} = \hat{H}_{\rm HFS} + \hat{H}_{\rm E}$, with

$$\hat{H}_{\rm HFS} = A_{\rm HFS}\hat{\mathbf{I}}\cdot\hat{\mathbf{J}} + B_{\rm HFS}\frac{3(\hat{\mathbf{I}}\cdot\hat{\mathbf{J}})^2+\frac{3}{2}\hat{\mathbf{I}}\cdot\hat{\mathbf{J}}-I(I+1)J(J+1)}{2IJ(2I-1)(2J-1)}, \quad (2)$$

where $\hat{\mathbf{I}}$ is the nuclear spin. The magnetic-dipole and electric-quadrupole hyperfine constants, $A_{\rm HFS}$ and $B_{\rm HFS}$, are well known for Rb [6,7].

We measure α_0 and α_2 using Rydberg two-photon excitation spectroscopy. The data analysis is based on linear fits of spectral data sets in a modified ac Stark map, in which the frequencies of the two excitation lasers are plotted against each other, with the unknown polarizabilities as fitting parameters. Our method does not require a precise calibration of the 1064-nm laser intensity at the atom trapping site. Also, light shifts are in the range of several gigahertz, which is important for a precise measurement of α_0 and α_2 of Rb $5P_{3/2}$ (level width 6 MHz).

We utilize an in-vacuum near-concentric cavity [see Fig. 1(a)] at 1064 nm to generate deep optical-lattice potentials in a linearly polarized field (finesse ≈ 600; for details see Ref. [8]). We load the lattice at low intensity directly from a ^{87}Rb magneto-optical trap (MOT). After the MOT light is pulsed off [for timing see Fig. 1(b)], a sinusoidal lattice-intensity ramp compresses the atom distribution in the lattice wells and increases the light shifts to several gigahertz. During the loading phase, the $5S_{1/2}$ ground-state atoms have a trap frequency of ≈ 700 kHz along Z and ≈ 7 kHz along X and Y. Hence, the 30 μs lattice ramp leads to adiabatic compression in the Z and mixed adiabatic-diabatic compression in the transverse directions. Atoms are excited into Rydberg states while the lattice is at high intensity. Rydberg atoms are detected by field ionization [9] and ion counting.

The lattice cavity is stabilized to the 1064-nm trap laser (short-term bandwidth 100 kHz) by the Pound-Drever-Hall (PDH) scheme [10] [see Fig. 1(c)]. The electro-optic modulator generates PDH frequency sidebands. The reflection from the cavity is sampled by a beam sampler for synthesizing the PDH error signal. The PDH feedback circuit has two outputs: a high-voltage slow feedback is applied to a piezo, which translates one of the cavity mirrors, and a fast feedback frequency modulates the acousto-optic modulator (AOM), which compensates the rapid frequency fluctuations of the trap laser. The lattice intensity ramp is generated by amplitude modulating the AOM. Our method to stabilize the optical cavity at high intracavity power differs from the strong-weak beam method [11] and from methods that use a separate reference cavity [12].

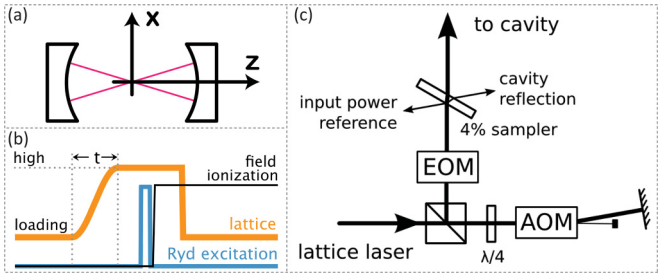

FIG. 1. (Color online) Experimental details. (a) A near-concentric cavity, which has a focus at its center, generates a gigahertz-deep 1064-nm optical-lattice laser trap. (b) Timing sequence showing lattice intensity, Rydberg excitation, and field ionization pulses vs time (lattice rise time $t = 30\ \mu$s, repetition rate = 100 Hz). (c) Key components of the Pound-Drever-Hall cavity stabilization. The error signal is normalized by an input power reference.

The polarizabilities are derived from two-photon stepwise (resonant) excitation signals from the light-shifted $5S_{1/2}$ ground state through a light-shifted $5P_{3/2}$ sublevel into the $74S_{1/2}$ Rydberg state. The two-photon excitation spectra are taken for a set of fixed lower-transition detunings, $\Delta_{\rm red}$, by recording Rydberg counts as a function of the upper-transition detuning, $\Delta_{\rm blue}$. We reference $\Delta_{\rm blue}$ to a narrow spectral line that corresponds to off-resonant two-photon excitation of Rydberg atoms outside the lattice. The detuning $\Delta_{\rm red}$ is referenced to the field-free $5S_{1/2}\,F = 2 \rightarrow 5P_{3/2}\,F' = 3$ transition. The spectra are arranged in waterfall plots in which the y coordinate is given by $\Delta_{\rm red}$, while $\Delta_{\rm blue}$ is plotted along the x axis. In Fig. 2 we show such a modified ac Stark map

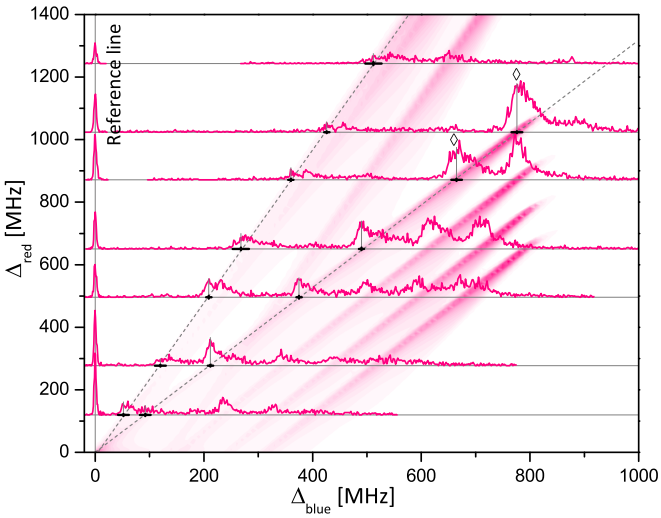

FIG. 2. (Color online) Experimental spectra (lines) vs the upper- and lower-transition detunings ($\Delta_{\rm blue}, \Delta_{\rm red}$), defined in the text. The gray drop lines mark the ($\Delta_{\rm blue}, \Delta_{\rm red}$) peak coordinates of the evaluated spectral lines. The bold crosses underneath the spectral lines indicate the uncertainties of the peak coordinates. The dashed lines show linear fits through the peak coordinates. In the background we show a simulated spectral-density plot (method explained in the text) for a lattice intensity 1.8×10^{11} W/cm^2, $\alpha_0(5P_{3/2}) = -1149.3$, $\alpha_2(5P_{3/2}) = 563.3$, and $\alpha_0(5S_{1/2}) = 687.3$ (polarizabilities in atomic units).

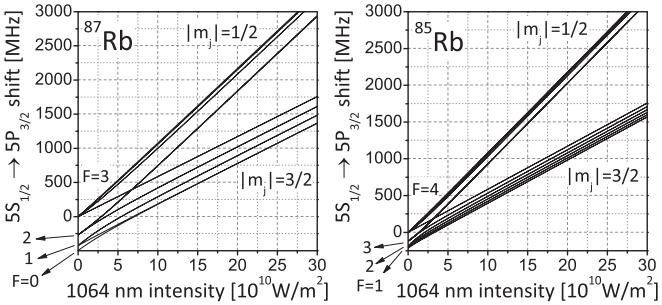

FIG. 3. ac Stark shifts of the transitions $5S_{1/2} \rightarrow 5P_{3/2}$ of ^{87}Rb(^{85}Rb) relative to the transition $5S_{1/2}, F = 2(3) \rightarrow 5P_{3/2}, F' = 3(4)$, calculated for $\alpha_0(5S_{1/2}) = 700$, $\alpha_0(5P_{3/2}) = -1100$, and $\alpha_2(5P_{3/2}) = 550$ atomic units.

measured for a transmitted lattice power of 20 mW, which corresponds to a peak intracavity intensity at the lattice sites of about 1.8×10^{11} W/m^2. The uncertainty of the transmitted lattice power is about 8% and that of the peak intracavity intensity is even larger. It is an essential advantage of our method that these uncertainties do not affect the values of α_0 and α_2 obtained from the data. This is because we derive α_0 and α_2 from slopes in the modified ac Stark map, not from absolute level positions. The self-referencing characteristics follow from the double-resonance condition under which both lower and upper transitions need to be on resonance to yield a signal. This allows us to express α_0 and α_2 in terms of the well-known polarizabilities of the ground and Rydberg states and measured level slopes. Also, reaching the regime in which light shifts are much larger than residual hyperfine shifts is important.

In Fig. 3 we show the light shifts of the $5S_{1/2} \rightarrow 5P_{3/2}$ transitions versus intensity, $I_0 = \frac{1}{2}c\epsilon_0 E_0^2$, calculated by diagonalization of $\hat{H}$ [see Eqs. (1) and (2)] using approximate values of α_0 and α_2. Since the $5S_{1/2}$ state has no a.ac-split sublevels, the splitting is only due to the $5P_{3/2}$ state, which has 16 sublevels for ^{87}Rb and 24 for ^{85}Rb. The plots exhibit three intensity regimes. In the weak-field regime, $\hat{H}_{\rm HFS}$ dominates, and $|F,m_F\rangle$ ($\hat{\mathbf{F}} = \hat{\mathbf{J}} + \hat{\mathbf{I}}$) is the "good" basis. Levels with the same F and $|m_F|$ values are degenerate, and their energy shifts are linear in intensity. At intermediate intensity neither $\hat{H}_{\rm HFS}$ or $\hat{H}_{\rm E}$ dominates, and the energy levels are generally nonlinear. The level crossing at 7×10^{10} W/m^2 (for ^{87}Rb) depends mostly on α_2 and the zero-field hyperfine splittings. For the determination of α_0 and α_2 we utilize the strong-field regime, which is analogous with the "Paschen-Back" regime of the Zeeman effect and is comfortably reached in our lattice cavity.

In the strong-field regime $\hat{H}_{\rm E}$ dominates, and $|IJm_Im_J\rangle$ is the "good" basis. The energy levels become linear functions of intensity again, and they separate into two groups of fixed $|m_J|$. Since $\alpha_2 > 0$, the group with higher (lower) energy includes levels with $|m_J| = \frac{1}{2}$ ($|m_J| = \frac{3}{2}$). Within each subgroup, the energies are split by the residual hyperfine perturbation. In the subspace $|m_J| = \frac{3}{2}$ the off-diagonal terms of $\hat{\mathbf{I}} \cdot \hat{\mathbf{J}}$ and $(\hat{\mathbf{I}} \cdot \hat{\mathbf{J}})^2$ vanish in the $|m_Im_J\rangle$ basis, and the residual hyperfine-induced shifts are given by the diagonal terms (for ^{87}Rb, $m_Im_J = \pm\frac{9}{4}$ or $\pm\frac{3}{4}$). Thus, the lower subgroups in Fig. 3 appear nearly equally spaced, due to the leading magnetic-dipole hyperfine term $A_{\rm HFS}\hat{\mathbf{I}} \cdot \hat{\mathbf{J}}$. The deviation from an equal spacing is due to the electric-quadrupole hyperfine term. In

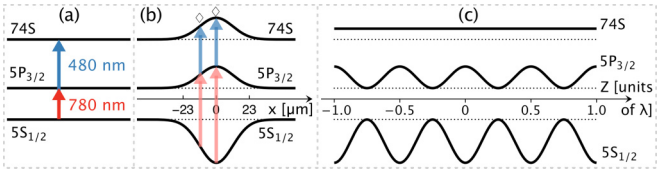

FIG. 4. (Color online) Relevant levels of the two-photon double-resonant Rydberg excitation. (a) Outside lattice. (b), (c) Light-shifted levels (solid lines) in transverse (b) and Z direction (c) in the 1064-nm lattice. The "magic" $74S$ state has a constant light shift along Z. Dotted lines indicate the unshifted levels. The intervals between levels are not to scale. The arrows illustrate several instances of doubly resonant excitation on one of the lines in Fig. 2 (see ◇ in Fig. 2).

the subgroups with $|m_J| = \frac{1}{2}$ the off-diagonal elements of $\hat{\mathbf{I}} \cdot \hat{\mathbf{J}}$ are generally nonzero, and the residual hyperfine shifts are not approximately equidistant. In our experiment we choose ^{87}Rb, because the number of m_I sublevels is less and the hyperfine splittings are larger than for ^{85}Rb.

The $5S_{1/2}$ and $5P_{3/2}$ levels exhibit a local response to the 1064-nm lattice light field, i.e., their light shifts are given by $-(\alpha/4)|E_0(\boldsymbol{R})|^2$, where $E_0(\boldsymbol{R})$ is the field amplitude at the center-of-mass location $\boldsymbol{R}$ of the atom. Due to their size, Rydberg atoms have a nonlocal response to the field [13,14]. The Rydberg-atom light shift is

$$V_{\rm ad}(\mathbf{R}) = -\frac{1}{4}\alpha_e \int |E_0(\mathbf{R}+\mathbf{r})|^2 |\psi(\mathbf{r})|^2 d^3r, \qquad (3)$$

where $\alpha_e = -545$ a.u. follows from the free-electron ponderomotive energy. Thus, the Rydberg-atom light shift is an average of the free-electron response, with the Rydberg electron's probability density $|\psi(\mathbf{r})|^2$ as a weighting factor. While generally $\psi(\mathbf{r})$ also depends on $\mathbf{R}$, for the nondegenerate nS Rydberg levels it is $\psi(\mathbf{r}) = \langle \mathbf{r}|nS\rangle$. In the z direction the averaging is important, because the size of the Rydberg atom is on the order of the lattice period, whereas in the ρ direction it is not, because the cavity-mode waist w_0 is much greater than the size of the Rydberg atom. For a few "magic" states, such as Rb $74S_{1/2}$ in a one-dimensional 1064-nm lattice, $V_{\rm ad}$ only depends on ρ and not on Z because the ratio of Rydberg-atom size and lattice period is such that the result of Eq. (3) does not depend on Z (see Supplemental Material [15]). For the magic states,

$$V_{\rm ad}(\rho, Z) = V_{\rm ad}(\rho) = -\frac{1}{4}\frac{\alpha_e}{2} E_{\rm max}^2 \exp\left(\frac{-2\rho^2}{w_0^2}\right), \qquad (4)$$

where $E_{\rm max}$ is the peak field amplitude in the entire lattice. In Fig. 4 we show the position dependence of the relevant light shifts as a function of atomic center-of-mass coordinates X and Z. The peaks in Fig. 2 correspond to doubly resonant excitation of $74S_{1/2}$ through one of the multiple $5P_{3/2}$ sublevels.

The density plot in the background of Fig. 2 shows the result of a simulation. The simulation accounts for the center-of-mass thermal distribution of the atoms in the optical lattice (temperature T), which causes most of the spectral line broadening. Doppler shifts are negligible and are ignored. The simulated count rate is an integral over the lattice volume that includes the Boltzmann factor, $\exp\{-\alpha_{5S}[E_{\rm max}^2 - E_0^2(\rho,Z)]/(4k_{\rm B}T)\}$, and the lower-transition saturation parameter, $0.5s/[1 + s + 4(\frac{\Delta}{6\ \rm MHz})^2]$. There, $s = I/I_{\rm sat}$ with saturation intensity $I_{\rm sat}$ and

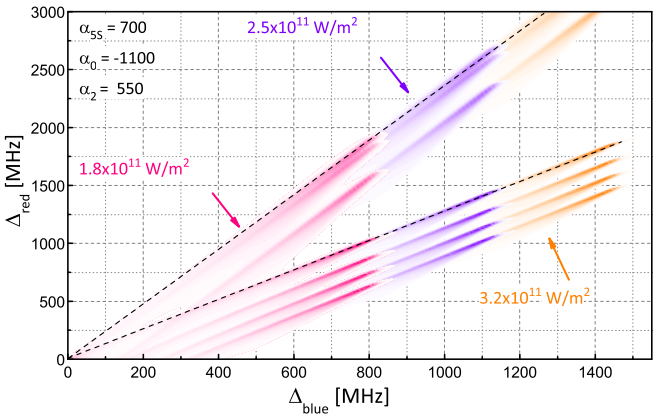

FIG. 5. (Color online) Simulated spectral-density Stark maps. We overlay three calculations for the indicated lattice intensities. The dashed lines indicate the levels and slopes used to determine α_0 and α_2 for the $5P_{3/2}$ level. The lower level is twofold degenerate (states $|m_J = 3/2, m_I = 3/2\rangle$ and $|m_J = -3/2, m_I = -3/2\rangle$), while the upper level is nondegenerate [state $(|m_J = 1/2, m_I = -1/2\rangle + |m_J = -1/2, m_I = 1/2\rangle)/\sqrt{2}$ in the high-field limit].

position-dependent intensity I. Also, Δ is the detuning of the 780 nm laser from the light-shifted, position-dependent $5S_{1/2} \rightarrow 5P_{3/2}$ transition frequency. The simulated count rate is summed over all intermediate $5P_{3/2}$ states. Figure 5 shows a compilation of three simulations for ^{87}Rb for different peak lattice intensities, $I_{\rm max}$, and the same polarizabilities. The slopes in the modified ac Stark map are insensitive to $I_{\rm max}$. The value of $I_{\rm max}$ affects the signal strength and the $\Delta_{\rm blue}$ cutoff, where the doubly resonant excitation condition is met at the field maxima (which are at locations $\rho = 0$ and $Z = k \times 532$ nm with integer k) for all $5P_{3/2}$ sublevels. While we can estimate $I_{\rm max}$ from the $\Delta_{\rm blue}$ cutoff, it is not required to determine the polarizabilities.

The lattice-shifted spectral lines are asymmetric and triangular due to the variation of the Rydberg light shift along surfaces of fixed intensity. This variation is due to the nonlocal response following Eqs. (3) and (4) (for a detailed discussion see [15]). We use the positions $(\Delta_{\rm blue}, \Delta_{\rm red})$ of the spectral-line peaks as primary markers, as shown in Fig. 2. These peaks correspond to combinations of intensity I, $\Delta_{\rm blue}$ and $\Delta_{\rm red}$ for which the double-resonance condition for exciting $74S_{1/2}$ is met at locations $Z = k \times 532$ nm with integer k [15].

In the modified ac Stark map, the peak positions $(\Delta_{\rm blue}, \Delta_{\rm red})$ satisfy

$$y = \Delta_{\rm red} = \Delta_{5S5P} = \frac{1}{4}(\alpha_{5S} - \alpha_{5P})E_0^2(\rho, Z=0),$$

$$x = \Delta_{\rm blue} = \Delta_{74S} + \Delta_{5S5P} - \Delta_{5P}$$

$$= \Delta_{5S5P} + \frac{1}{4}(\alpha_{5P} - \alpha_{74S})E_0^2(\rho, Z=0) = y\frac{\alpha_{5S} - \alpha_{74S}}{\alpha_{5S} - \alpha_{5P}},$$

where $E_0(\rho, Z=0)$ is the maximal lattice field at a distance ρ from the axis. The slopes of the levels are independent of E_0 and are

$$\frac{dy}{dx} = \frac{\alpha_{5S} - \alpha_{5P}}{\alpha_{5S} - \alpha_{74S}}. \qquad (5)$$

TABLE I. Experimental $5P_{3/2}$ scalar and tensor polarizabilities in 1064-nm light field. The uncertainties are reading and fitting uncertainties. Polarizabilities are in atomic units.

Parameter	Value	Uncertainty
Experimental slope $\lvert m_j\rvert = \frac{3}{2}$	1.33	4.19×10^{-3}
Experimental slope $\lvert m_j\rvert = \frac{1}{2}$	2.50	4.47×10^{-2}
Differential slope	1.17	4.49×10^{-2}
Average slope	1.91	2.24×10^{-2}
α_0 (experiment)	−1149	22
α_2 (experiment)	563	22
α_0 (theory [16])	−1121	10
α_2 (theory [16])	551	4

In the high-field (Paschen-Back) regime, the polarizabilities for the highest energy levels within the subgroups $|m_j| = \frac{1}{2}$ and $|m_j| = \frac{3}{2}$ are given by $\alpha_{5P} = \alpha_0 \mp \alpha_2$, respectively. Their differential and average slopes are

$$\left.\frac{dy}{dx}\right|_{|m_j|=1/2} - \left.\frac{dy}{dx}\right|_{|m_j|=3/2} = \frac{2\alpha_2}{\alpha_{5S} - \alpha_{74S}}, \tag{6}$$

$$\frac{1}{2}\left(\left.\frac{dy}{dx}\right|_{|m_j|=1/2} + \left.\frac{dy}{dx}\right|_{|m_j|=3/2}\right) = \frac{\alpha_{5S} - \alpha_0}{\alpha_{5S} - \alpha_{74S}}. \tag{7}$$

The slopes dy/dx are determined by linear fitting of the sets of peaks $(\Delta_{\text{blue}}, \Delta_{\text{red}})$ associated with the respective lines in the modifiedac Stark map. For $|m_j| = \frac{3}{2}$ we force the y intercept to zero because this level has a fixed slope through all field regimes and passes through the origin. For $|m_j| = \frac{1}{2}$ we fit both the slope and the intercept. This is because in the weak-field regime the $|m_j| = \frac{1}{2}$ level connects to $|F = 3, m_F = 0\rangle$, which has $\alpha_{5P} = \alpha_0 - \frac{4}{5}\alpha_2$. Hence, the high-field fit of the $|m_j| = \frac{1}{2}$ level yields a slight negative y intercept (about −30 MHz for $I_{\max} = 1.8 \times 10^{11}$ W/m^2). We fit the slopes for measurements at several values of $I_{\max}$ and excitation-pulse durations [15]. The weighted average slopes are summarized in Table I. The α_{5S} and α_{74S} are, for the present purpose, precisely known [$\alpha_{5S} = 687.3(5)$ [16] and $\alpha_{74S} = -272.5(5)$ [13,15], in atomic units]. Equations (6) and (7) then yield $\alpha_0 = -1149$ and $\alpha_2 = 563$ a.u.

The uncertainties listed in Table I only reflect the linear-fitting uncertainty and the reading uncertainties associated with the determination of the peak coordinates $(\Delta_{\text{blue}}, \Delta_{\text{red}})$. The calibration uncertainties for Δ_{blue} and Δ_{red} are 1.6% and 0.2%, respectively. Adding all relative uncertainties in quadrature, the final uncertainties are 2.5% for α_0 and 4.2% for α_2 [15]. Our result is in good agreement with theoretical values $\alpha_0 = -1121(10)$ and $\alpha_2 = 551(4)$ obtained in Ref. [16]. Also, we have adopted the theoretical calculation of $\alpha_{5S} = 687.3(5)$ in [16], instead of an earlier calculation from [17] and an experimental value $\alpha_{5S} = 769(61)$ [18].

A different approach to polarizability measurement in 1064-nm laser fields can be found in [19]. Also, in related work [20] the breakdown of the hyperfine coupling is studied in fields up to about $\sim 2 \times 10^{10}$ W/m^2 (about ten times less than in the present work), with similar polarizability results. There, theoretical polarizabilities for both $5S_{1/2}$ [16] and $5P_{1/2}$ are required to calibrate the laser electric field and to then infer experimental values for the $5P_{3/2}$ polarizabilites.

The scalar and tensor polarizabilities of $5P_{3/2}$ are immediately useful in experiments that require on-resonant transitions through $5P_{3/2}$, such as two-photon preparation of lattice-mixed hydrogenic Rydberg states in deep 1064-nm lattices [21], Rydberg-EIT in 1064-nm optical traps, and evaporative cooling utilizing 1064-nm light fields. The double-resonance, self-referencing, Rydberg-based method to measure atomic polarizabilities could be adapted for other atoms in a variety of optical traps and at different wavelengths, such as for Cs in a deep 1064-nm optical lattice or dipole trap, or for Rb in a high-power CO_2-laser trap. Instead of using a magic Rydberg state, one may utilize low-lying Rydberg states that are sufficiently small that they exhibit an approximately local response to the field (given by the free-electron polarizability, $\alpha_e = -545$).

We thank B. K. Sahoo for providing theoretical values of scalar and tensor polarizabilities, and M. S. Safronova for helpful discussions. L.F.G. acknowledges São Paulo Research Foundation (FAPESP) Grant No. 2014/09369-0. This work is supported by NSF Grant No. PHY-1205559.

[1] S. G. Porsev, K. Beloy, and A. Derevianko, Phys. Rev. Lett. **102**, 181601 (2009).
[2] D. Jiang, B. Arora, M. S. Safronova, and C. W. Clark, J. Phys. B: At., Mol. Opt. Phys. **42**, 154020 (2009).
[3] V. A. Dzuba, J. C. Berengut, V. V. Flambaum, and B. Roberts, Phys. Rev. Lett. **109**, 203003 (2012).
[4] Bindiya Arora, M. S. Safronova, and C. W. Clark, Phys. Rev. A **76**, 052509 (2007).
[5] E. A. Goldschmidt, D. G. Norris, S. B. Koller, R. Wyllie, R. C. Brown, J. V. Porto, U. I. Safronova, and M. S. Safronova, Phys. Rev. A **91**, 032518 (2015).
[6] D. A. Steck, Rubidium 85 D Line Data, available online at http://steck.us/alkalidata (revision 2.1.6, 20 September 2013).
[7] D. A. Steck, Rubidium 87 D Line Data, available online at http://steck.us/alkalidata (revision 2.1.4, 23 December 2010).
[8] Yun-Jhih Chen, Stefan Zigo, and Georg Raithel, Phys. Rev. A **89**, 063409 (2014).
[9] T. F. Gallagher, *Rydberg Atoms* (Cambridge University Press, Cambridge, 1994).
[10] E. D. Black, Am. J. Phys. **69**, 79 (2001).
[11] P. D. Edmunds and P. F. Barker, Rev. Sci. Instrum. **84**, 083101 (2013).
[12] P. Hamilton, M. Jaffe, J. M. Brown, L. Maisenbacher, B. Estey, and H. Müller, Phys. Rev. Lett. **114**, 100405 (2015).
[13] S. K. Dutta, J. R. Guest, D. Feldbaum, A. Walz-Flannigan, and G. Raithel, Phys. Rev. Lett. **85**, 5551 (2000).
[14] T. Topcu and A. Derevianko, Phys. Rev. A **88**, 043407 (2013).
[15] See Supplemental Material at http://link.aps.org/supplemental/10.1103/PhysRevA.92.060501 for additional experimental data sets, discussions of the Rydberg-state polarizability and the spectroscopic line shapes, and a detailed uncertainty analysis.

[16] Bindiya Arora and B. K. Sahoo, Phys. Rev. A **86**, 033416 (2012), and private communication.
[17] M. Marinescu, H. R. Sadeghpour, and A. Dalgarno, Phys. Rev. A. **49**, 5103 (1994).
[18] K. D. Bonin and M. A. Kadar-Kallen, Phys. Rev. A **47**, 944 (1993).
[19] P. D. Edmunds and P. F. Barker, Phys. Rev. Lett. **113**, 183001 (2014).
[20] A. Neuzner, M. Körber, S. Dürr, G. Rempe, and S. Ritter, Phys. Rev. A **92**, 053842 (2015).
[21] K. C. Younge, S. E. Anderson, and G. Raithel, New J. Phys. **12**, 023031 (2010).